Electronic Supplementary Material (ESI) for Materials Horizons.

Supporting Information

A Simple Route to Functionalized Porous Carbon Foams from Carbon Nanodots for Metal-free Pseudocapacitors

Experimental Section

Solid-state synthesis of CNDs and SCNDs: All chemicals mentioned were incorporated in the procedure as purchased (i.e., without processing or purification). Carbon nanodots (CNDs) were synthesized by means of solid-state pyrolysis of urea and citric acid in argon flow. Preparation of SCND precursor solution involved dissolving 18 mmol citric acid (Fisher Scientific, ACS grade), 3.6 mmol urea (Aldrich, 99%), and 1.6 mmol sulfanilic acid (4-aminobenzenesulfonic acid, Fisher Scientific, ACS grade) in 300 mL deionized water. To acquire a homogeneous precursor for the solid-state reaction, this solution went through freeze-drying at -40 °C. The freeze-dried precursor was then moderately ground down to grains ready for pyrolysis using a pestle and a mortar. Under a 250 mL min^{-1} Ar flow, a tube furnace heated the precursor to 300 °C at 10 K min^{-1}. The sample was held at this temperature for 2 hours and then cooled to room temperature. Following this, the product was collected, dispersed in 100 mL deionized water under ultrasonication, and centrifuged at 4750 rpm for 30 min. To remove unreacted reactants, the supernatant went through dialysis in regenerated cellulose dialysis tubing with MWCO 1k Da for 48 h to remove unreacted reactants. Once more, the remaining aqueous solution was freeze-dried for later characterization and application steps. Pyrolysis at a temperature gradient was carried out in a range from 220 to 400 °C. The SCNDs with different graphitization degrees were obtained.

Laser Formation of 3D-tsSC electrodes: The dried SCND powder (formed at temperature gradient) was dispersed in ethylene glycol at 10 mg/mL and drop-casted on stainless steel. Hydrophilic tapes were used to help control and enclose the drop cast area. A film, upon baking at 70 °C, was formed at a density of 0.5 mL/cm^2 at the pyrolytic graphite sheet (Digi-Key Corporation, 0.07 mm). The baked film was irradiated with a CO_2 laser (Full Spectrum FSL laser engraver, 10.6 μm). The laser was set to 30% of its 45W full power and 30% of its max scan speed (~9 cm s^{-1}). The Z height was adjusted to focus on the top surface of the coating film. A 50 mm diameter zinc selenide window was incorporated into the reaction chamber lid, allowing the CO_2 laser (10.6 μm) to pass into the gas-reaction chamber. The sample was placed in the center of the chamber. A continuous airflow of 0.1 L s^{-1} during the reaction was used to ensure good mass transfer. The substrate-supported films were washed by immersing them into either NMP or 1.0 M KOH. After the unreacted SCND was dissolved, the electrodes were thoroughly rinsed with deionized water and methanol. The resulting film was used as the electrodes for the electrochemical characterizations.

Fabrication of high-mass loading 3D-tsSC electrodes: Electrodes were fabricated through repeated drop-cast and laser conversion processes. On the top of the first layer of 3D-tsSC laser formation, a certain number of sequential drop casts was done at the same loading density. Each drop cast was followed by a laser conversion at the same power and speed settings. The thickness was determined by averaging the distance in cross-sectional SEM images at three spots. The electrode loading mass was determined by the final mass subtracting the mass of graphite paper. The average mass loadings were measured by averaging five electrodes (1 cm^2): 0.39 mg cm^{-2} was obtained after a single 1-layer deposition-laser: 0.76 mg cm^{-2} was obtained after a 2-layer deposition-laser: 1.05 mg cm^{-2} was obtained after a 3-layer deposition-laser: 2.21 mg cm^{-2} was obtained after a 5-layer deposition-laser; and 5.7 mg cm^{-2} was obtained after a 10-layer deposition-laser.

Assembly of Flexible all-solid-state 3D-tsSC Supercapacitors (3D-tsSC FSSCs): The symmetric device contains a 1.0 M H_2SO_4 gel electrolyte. The preparation of which involved dissolving 1.0 g PVA in 10 mL water, stirred vigorously for 30 min at 90 °C, to which 0.56 mL of stock H_2SO_4 was added. The electrolyte was then deposited at the surfaces of two 3D-tsSC electrodes (2 cm x 2 cm) and left to rest for 1 h to ensure surface wetting. A cellulose separator (NKK TF4030) was next placed between the two electrodes to assemble the device. The device was dried for 12 h at room temperature until the gel solidified. After drying the FSSC was sealed with Kapton tape on both sides to prevent the electrolyte loss during the electrochemical characterizations.

Electrochemical characterization: The electrochemical characterizations were performed on a Biologic VMP3 electrochemical workstation. The three-electrode characterization was performed using 3D-tsSC as the working electrode, graphite sheet as the counter electrode, and a standard Ag^+/AgCl (1M KCl) as the reference electrode. The two-electrode characterization was performed using 3D-tsSC as both working and counter electrodes. For CV and GCD studies, the window voltages were set from 0 to 1.0 V. Specifically in three-electrode configuration, the potential was set as -0.2 to 0.8 V vs. Ag^+/AgCl reference electrode, which can be converted to 0 to 1.0 V vs. standard hydrogen electrode (SHE). The cycling stability test was carried out using a GCD method. EIS tests were performed at 10 mV amplitude in the frequency range from 10 mHz to 100 000 Hz. The OCV self-discharge processes were evaluated by the Biologic VMP3 electrochemical workstation. Specifically, the OCV self-discharge was measured via charging to a working voltage of 1.0 V with 0.1 A g^{-1} constant current density and maintaining a constant voltage for 120 min. Once the supercapacitor was fully charged, the circuit was disconnected and the change of open circuit voltage recorded with time to determine the self-discharge. In order to ensure the stability of the equipment and reduce the influence of charge redistribution on the self-discharge, 50 cycles of cyclic voltammetry were scanned at 200 mV s^{-1} before the leakage current and self-discharge test.

General characterization: A Jasco FT/IR-4100 with a single reflection ATR unit was used for FT-IR spectroscopy. Bruker's D8 Discover powder X-ray diffractometer recorded CuKα radiation (**λ**= 1.5406 Å) XRD patterns. A Renishaw InVia Raman Microscope with a 633 nm laser captured Raman spectra in individual spectral or mapping mode. Single Lorentzian functions with R2-values of 0.99 fit Raman spectra peak fitting. Fluorescence baseline subtraction and Lorentz peak centers deconvolved the powder Raman spectra. Peak positions were determined via Raman spectra of several materials. A 3 or 5 kV FEI Nova 230 Nano SEM was used for SEM. Al or Cu foil substrates were used to support samples. A 120 kV FEI T12 TEM performed TEM. A 5 μL ethanol-diluted powder dispersions were drop casted over Lacey-carbon supported TEM grids to produce TEM samples. A Kratos Axis Ultra DLD spectrometer with a monochromatic Al Kα X-ray source (hv = 1486.6 eV) produced XPS spectra. Carbon tape (Ted Pella) was used to calibrate high-resolution spectra. CasaXPS processed raw data (version 2.3.16). C 1s spectra were fit using Gaussian–Lorentzian line-shapes for all spectral components except the sp^2 C component, which was fitted with an asymmetric line shape to reflect the metallic nature of the samples. All samples used FWHM and position limitations for consistency. UPS measurements were performed on the same instrument with an unfiltered HeI (21.22 eV) gas discharge lamp and a total instrumental energy resolution of 100 meV. The electrical sheet conductivity of the 3D-tsSC electrodes was measured using the four-point conductivity probe (Veeco; Plainview, NY). The contact angles

were measured using the First Ten Angstroms contact angle analyzer Model FTA 125. The droplets were formed by 0.05 mL 1M H2SO4 water solution.

Methylene blue surface area determination: The surface area is determined using the powder collected and washed from the laser formation step. 50 mg of the powder is displaced in an aqueous solution of methylene blue with a concentration of 0.1 M. Note that polypropylene beakers and vials were used to handle methylene blue. The mixture is stirred vigorously for 24 h and is then centrifuged at 16,000 rpm to isolate any suspended material. The supernatant is measured in its absorption at 665 nm against a reference of the stock solution of 0.1 M aqueous methylene blue. The measurement also relied on the assumption that every methylene blue molecule occupies 1.35 nm^2 of active surface area.

Calculation of specific capacitance: Gravimetric specific capacitance (C_S) of electrodes tested in a two-electrode cell setup and areal capacitance (C_A) of FSSC symmetric devices were calculated from GCD profiles using the following relations:

$$C_S = 4 \times \frac{I \times \Delta t}{m \times \Delta V} \ (Fg^{-1}) \quad (1)$$

$$C_A = 2 \times \frac{I \times \Delta t}{A \times \Delta V} \ (Fcm^{-2}) \quad (2)$$

where I is the discharge current (mA), Δt the duration of discharge (s), m the active material mass loading (mg), A the surface area of the electrode (cm^2), and ΔV the voltage window (V).

Calculation of Coulombic efficiency based on GCD: Charge and discharge curves of the GCD profiles are integrated to yield total capacity charged and total capacity discharged, and the ratio of discharged capacity to charged capacity grants the Coulombic efficiency of particular electrodes/devices.

Energy density *E* and power density *P* follow the equations below:

$$E = \frac{1}{2} C_x \Delta V^2 \times \frac{1000}{3600} \ (Wh/kg) \quad (3)$$

$$P = \frac{E}{\Delta t} (Wh/kg) \quad (4)$$

where $C_x = C_S$ for the energy density of electrodes in the two electrode-configuration, outputting gravimetric energy density.

Calculation of Capacitance from Impedance: The electrode-electrolyte interface is approximated with a Randles circuit within the frequency range of 10 mHz to 100 Hz to estimate the real component of capacitance (C'). Electrochemical impedance spectroscopy provided impedance readings from which real and imaginary components of capacitance can be derived as follows:

$$C' = -Z'' / 2\pi f |Z|^2 \quad (5)$$

$$C'' = -Z' / 2\pi f |Z|^2 \quad (6)$$

where f represents the frequency (Hz), |Z| represents the absolute value of impedance, and Z' and Z'' represent, respectively, the real and imaginary impedance components.

With the real and imaginary impedance components, the phase angle may by calculated with the following equation:

$$\phi = -arctan(Z'(\omega)/Z''(\omega))$$

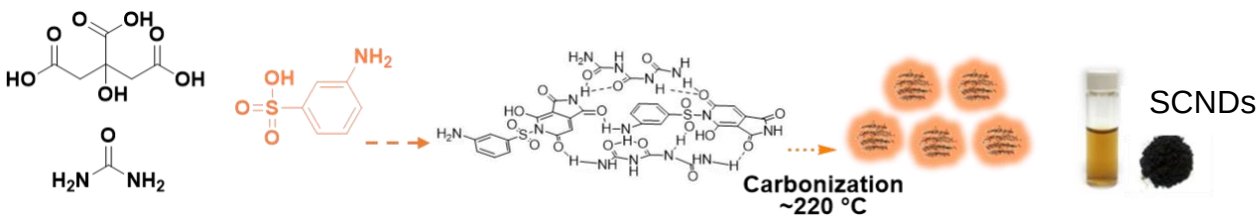

Figure S1 Reaction diagram of SCNDs formation.

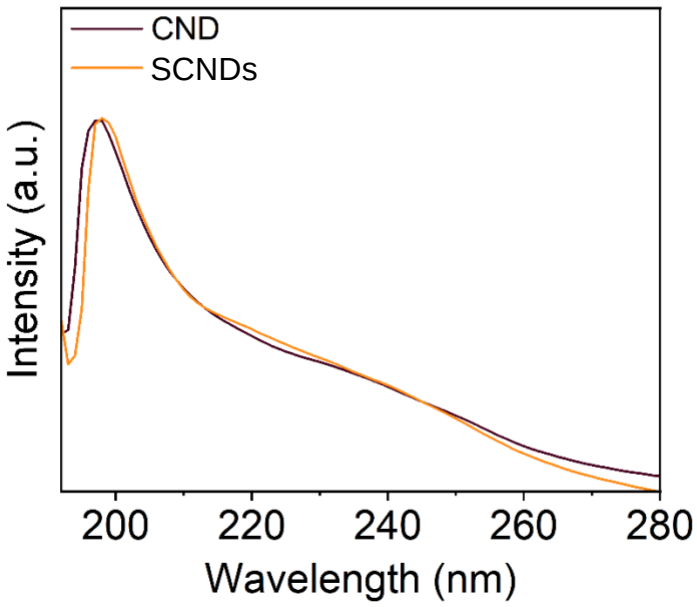

Figure S2 UV-vis spectrum of SCNDs and non-functionalized CNDs in ethanol solutions.

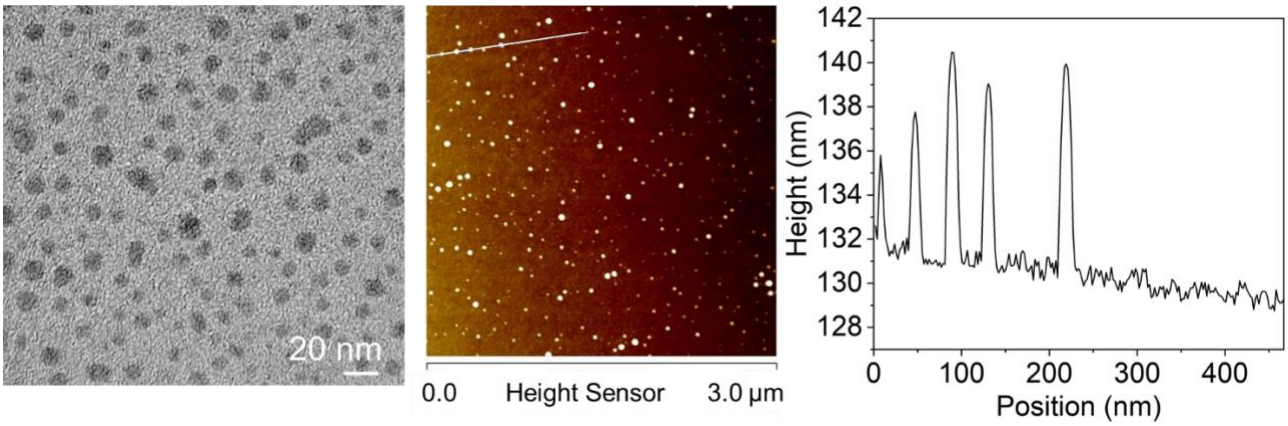

Figure S3 TEM (left) and AFM (middle) images of SCNDs. The height profile diagram indicates the sizes of five carbon SCNDs shown on the white line in the AFM image.

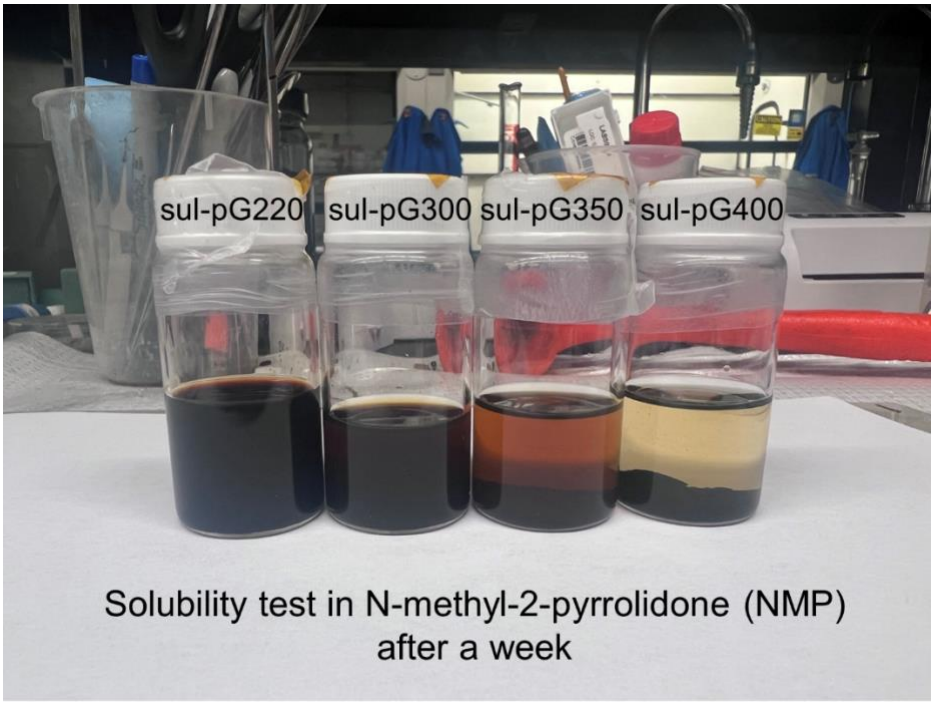

Figure S4 The dispersion of 3D-tsSC220, 3D-tsSC300, 3D-tsSC350, and 3D-tsSC400 in NMP after one week.

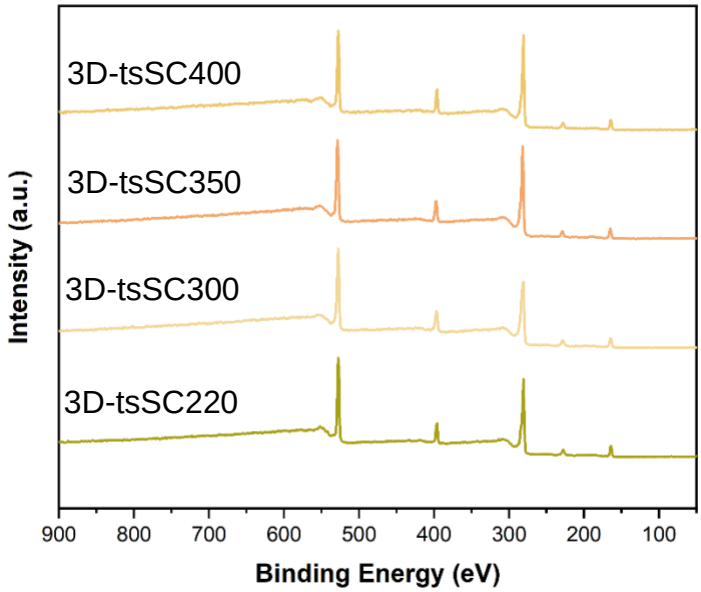

Figure S5 XPS survey spectrum of SCND220, SCND300, SCND350, and SCND400.

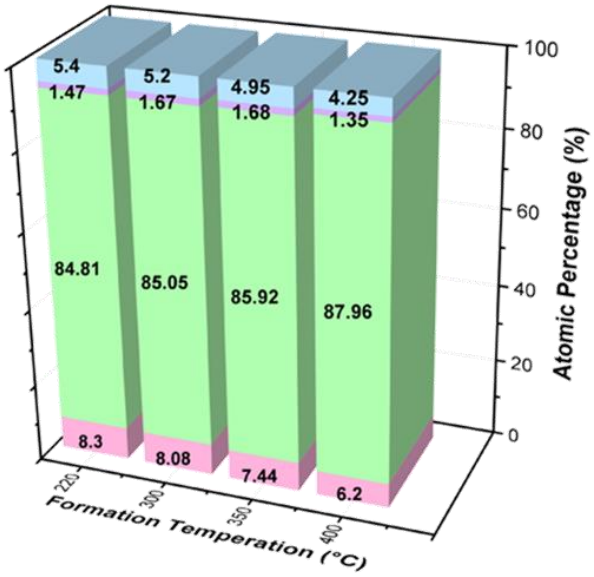

Figure S6 Compositional percentages of S2p, O1s, N1s, and C1s of SCND220, SCND300, SCND350, and SCND400 derived from their XPS survey spectra, respectively.

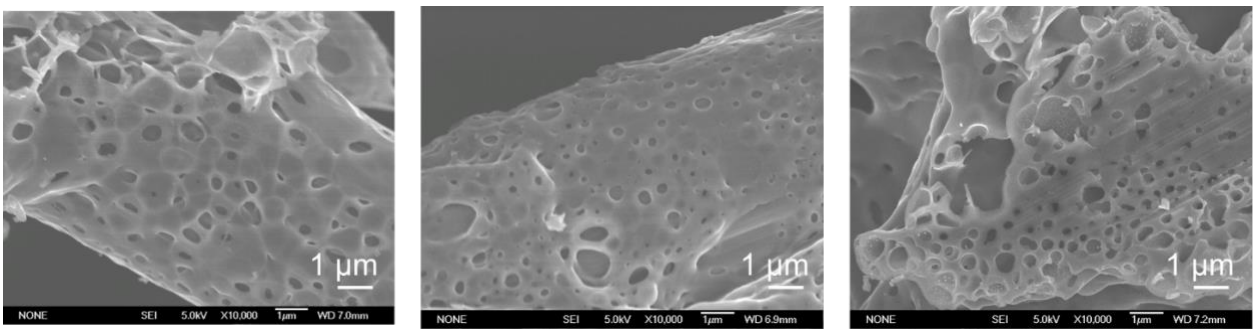

Figure S7 Typical SEM images of 3D-tsSC220 (left), 3D-tsSC350 (middle), and 3D-tsSC400 (right).

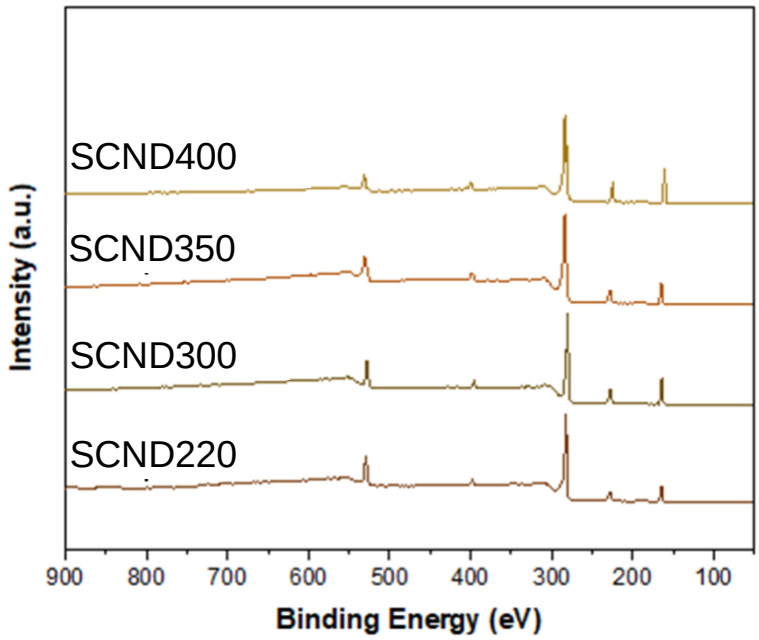

Figure S8 XPS survey spectrum of 3D-tsSC220, 3D-tsSC300, 3D-tsSC350, and 3D-tsSC400.

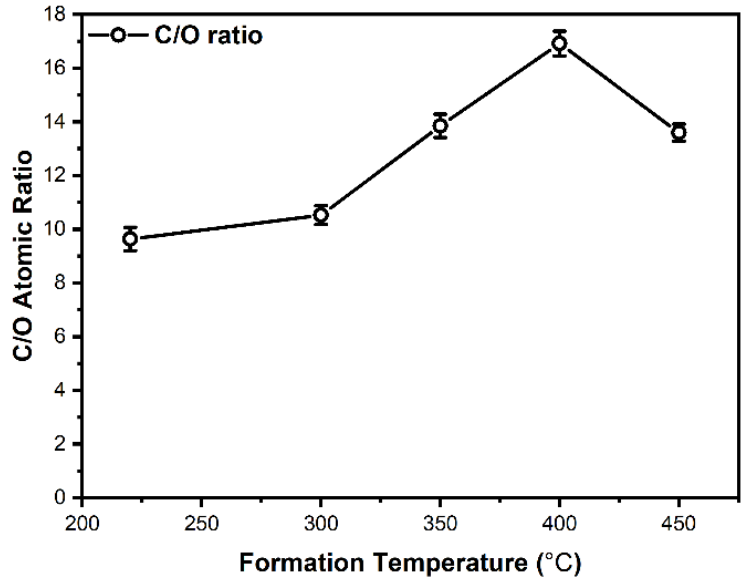

Figure S9 Variation of C/O ratios of 3D-tsSC220, 3D-tsSC300, 3D-tsSC350, 3D-tsSC400, and 3D-tsSC450.

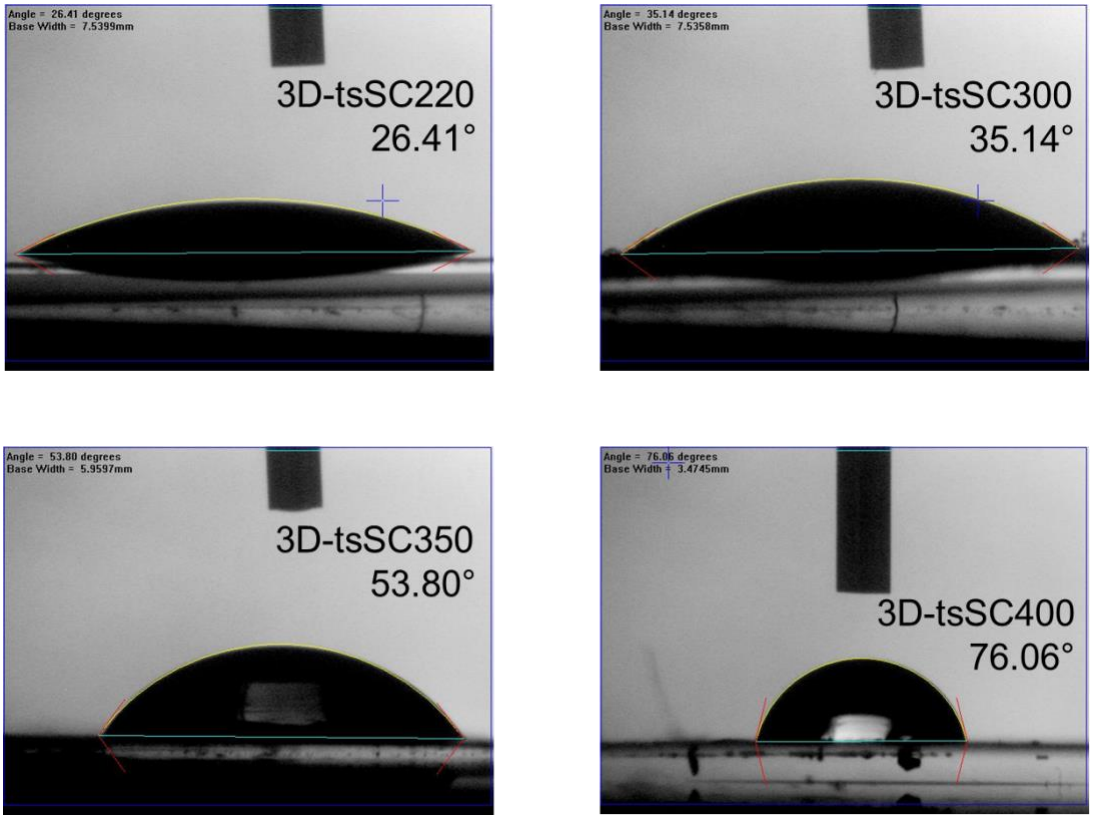

Figure S10 1M H_2SO_4 contact angles of 3D-tsSC220, 3D-tsSC300, 3D-tsSC350, and 3D-tsSC400.

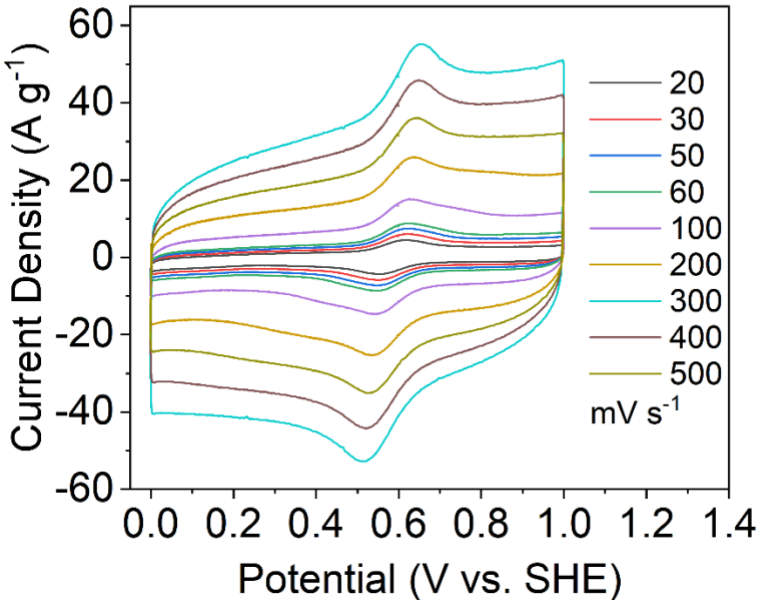

Figure S11 CV scans of 3D-tsSC300 at various scan rates in 1M H_2SO_4 measured by three-electrode configuration.

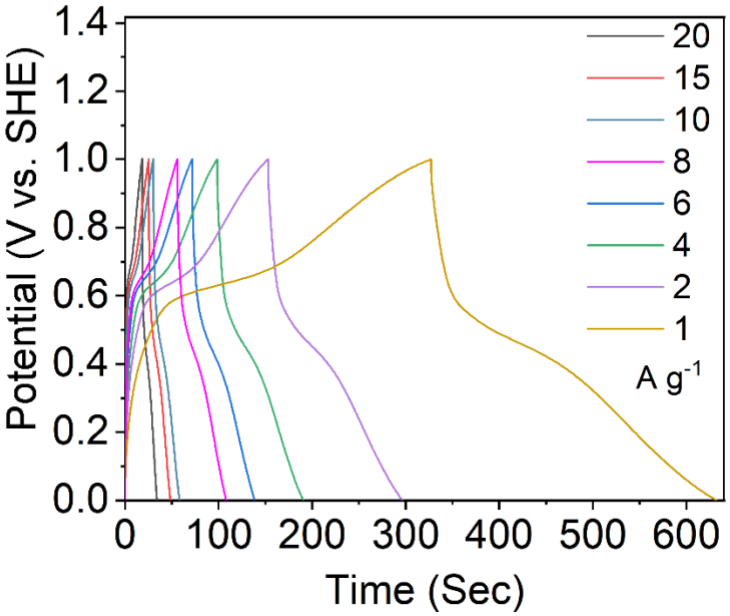

Figure S12 GCD profiles of 3D-tsSC300 at various current densities in 1M H_2SO_4 measured by three-electrode configuration.

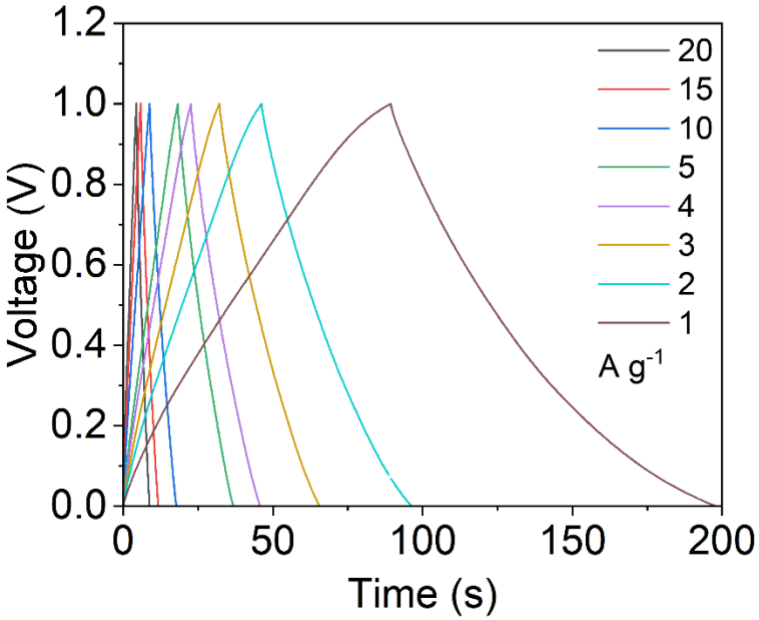

Figure S13 GCD profiles of tsSC at various current densities in 1M H_2SO_4 measured by three-electrode configuration.

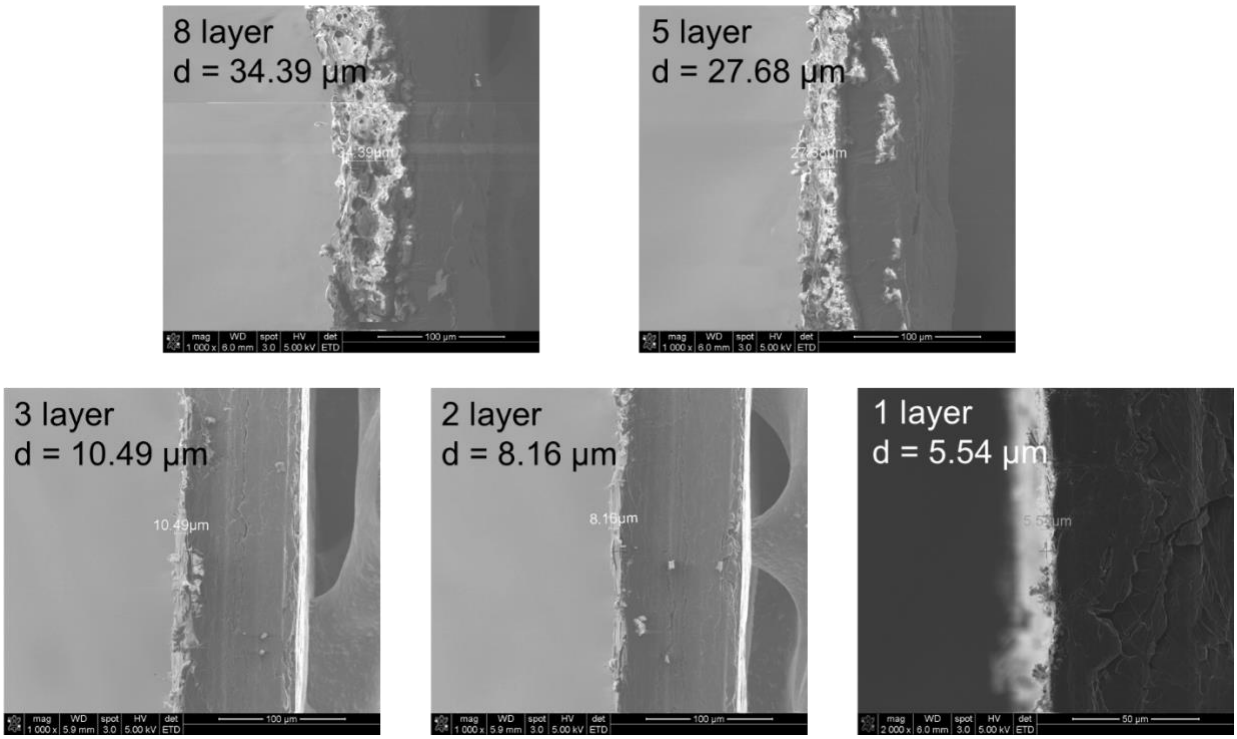

Figure S14 Cross-sectional SEM images and electrode thickness measurement of different loading masses.

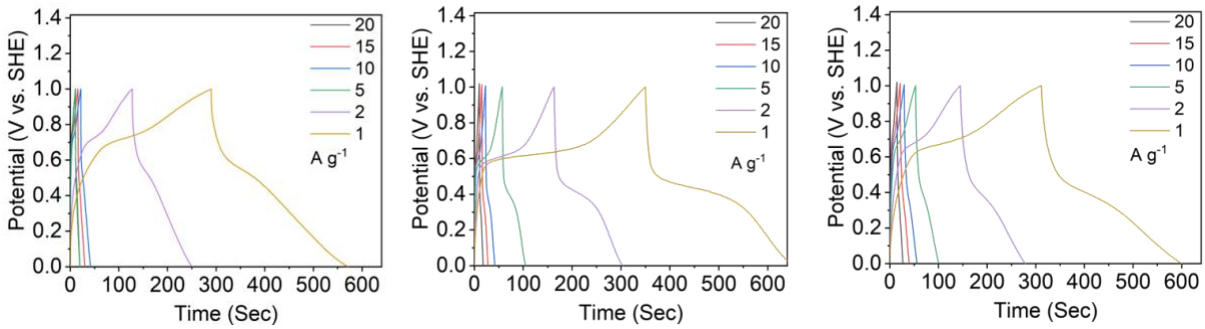

Figure S15 GCD profiles of 3D-tsSC220, 3D-tsSC350, and 3D-tsSC400 at various current densities in 1M H_2SO_4 measured by three-electrode configuration.

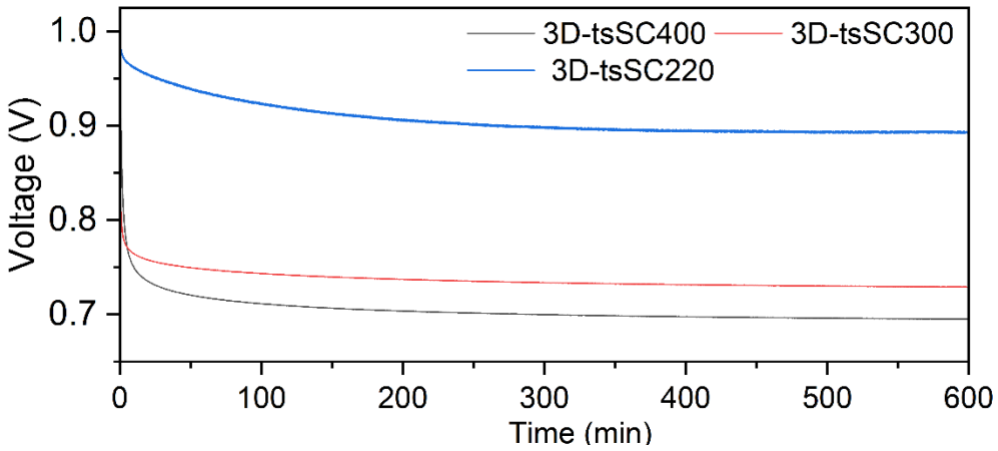

Figure S16 OCV self-discharge curve after charging at 1.0 V for 120 min.

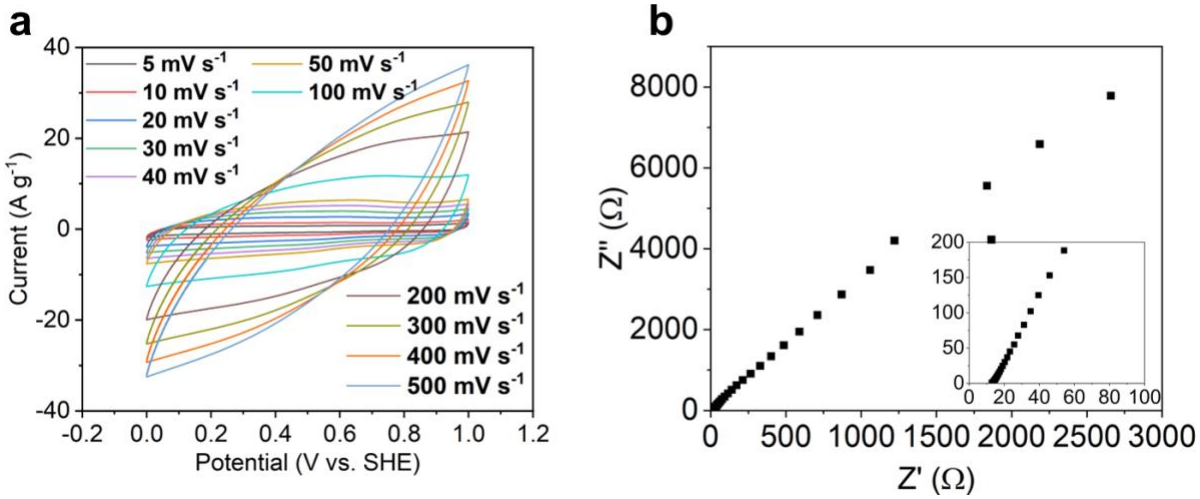

Figure S17 a) the CV profiles at various scan rates, b) the Nyquist plot (inset is a zoom-in plot in high frequency region) of 3D-tsSC300 in 1 M Na_2SO_4 aqueous electrolyte.

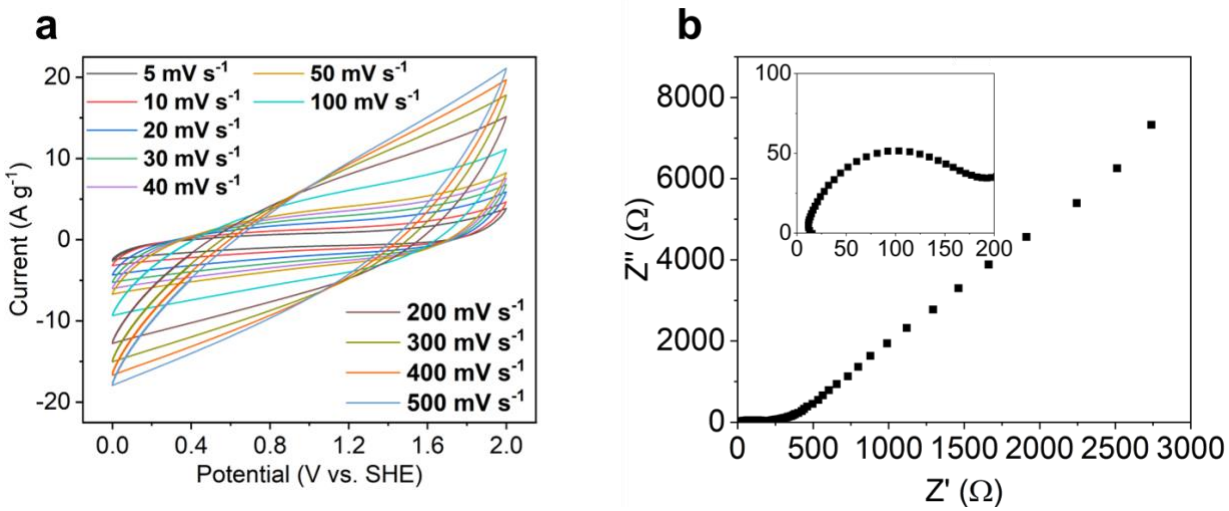

Figure S18 a) the CV profiles at various scan rates, b) the Nyquist plot (inset is a zoom-in plot in high frequency region) of 3D-tsSC300 in 0.5 M $TEABF_4$/ACN organic electrolyte.

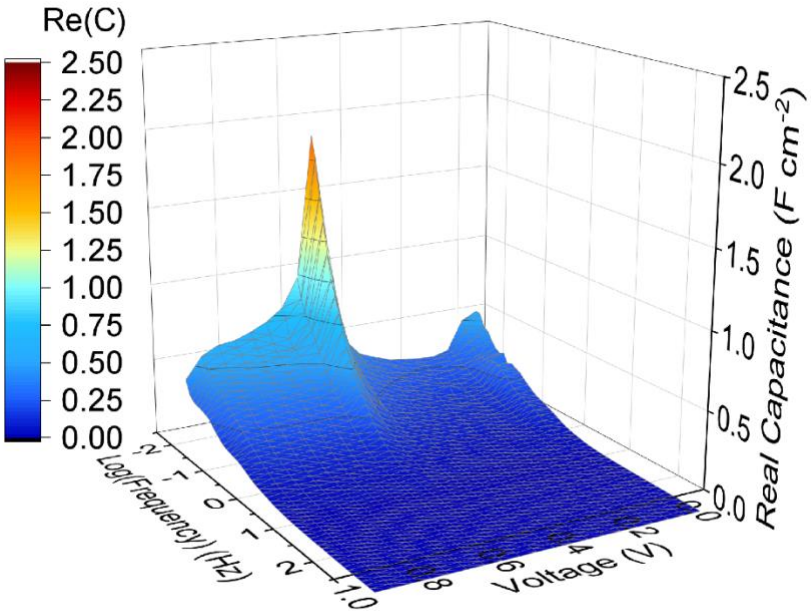

Figure S19 3D Bode plot of 8-layer 3D-tsSC220 electrode.

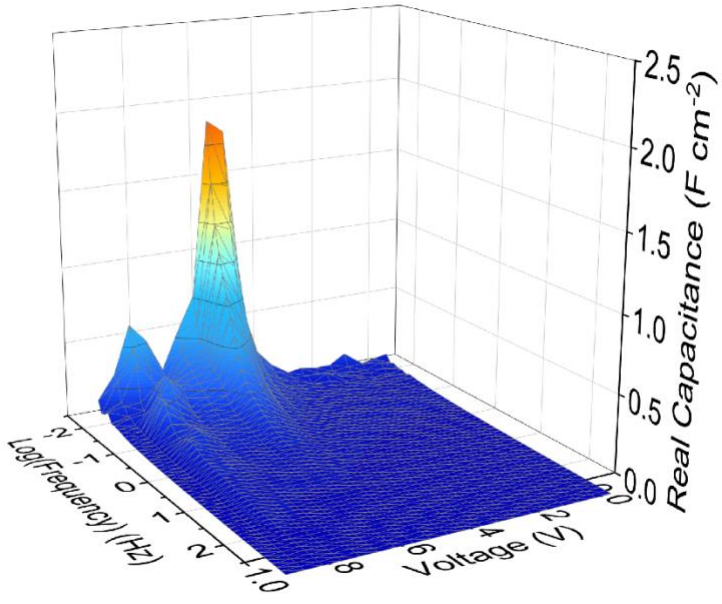

Figure S20 3D Bode plot of single layer 3D-tsSC300 electrode.

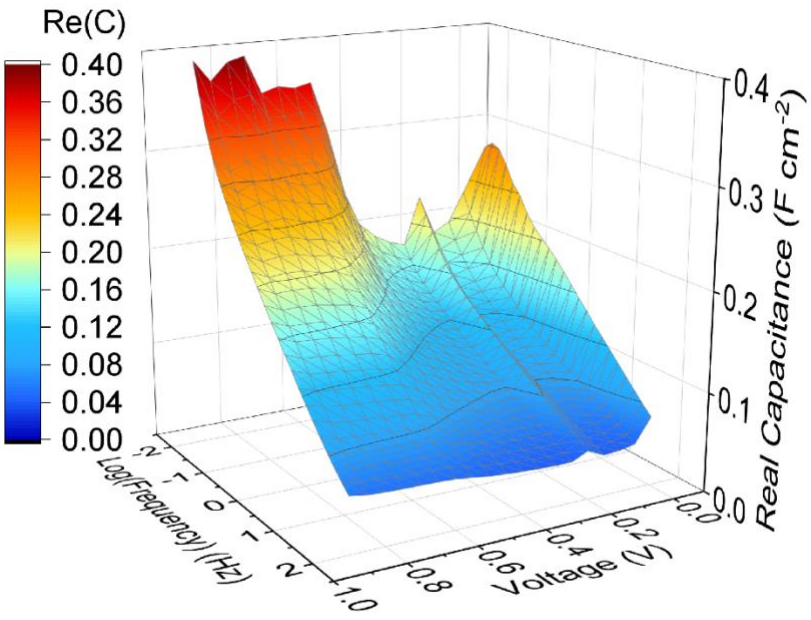

Figure S21 3D Bode plot of single layer unfunctionalized CND laser-converted tsSC electrode.

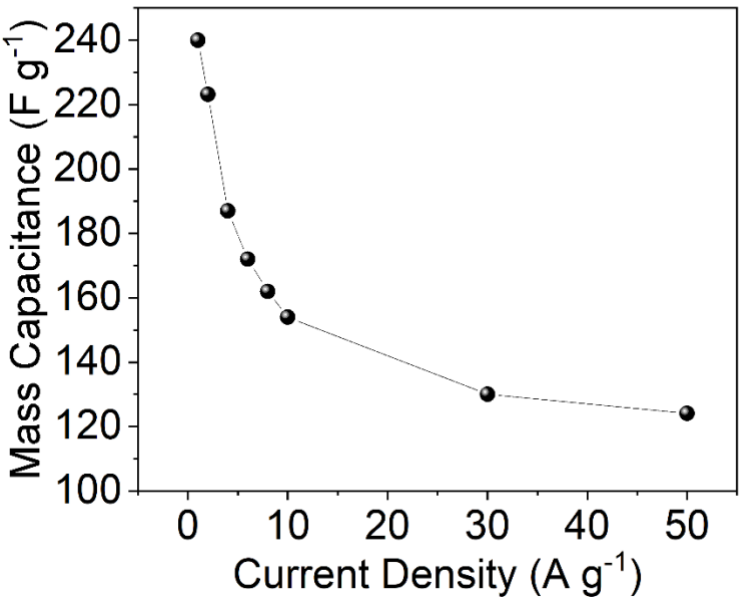

Figure S22 Mass capacitances of symmetric 3D-tsSC300 at various current densities.

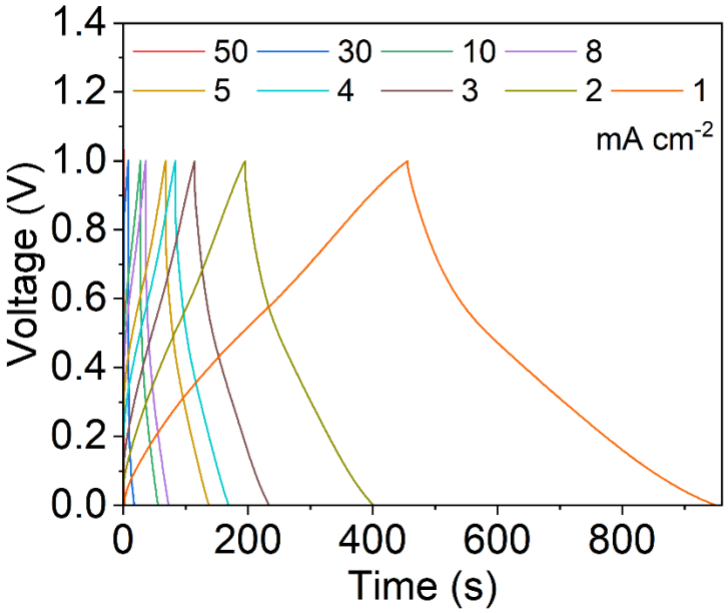

Figure S23 GCD plot of 3D-tsSC300 symmetric supercapacitor at various current densities.

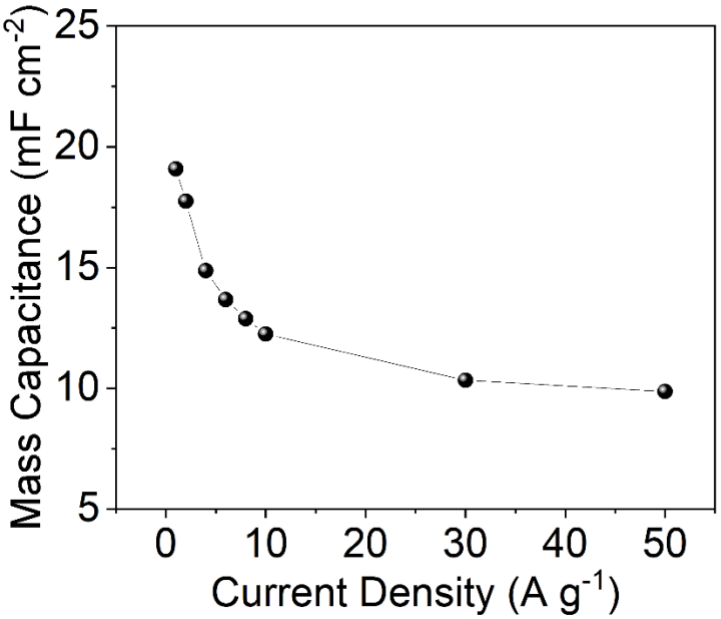

Figure S24 Rate performance of sup-pG300 FSSC at various current densities.

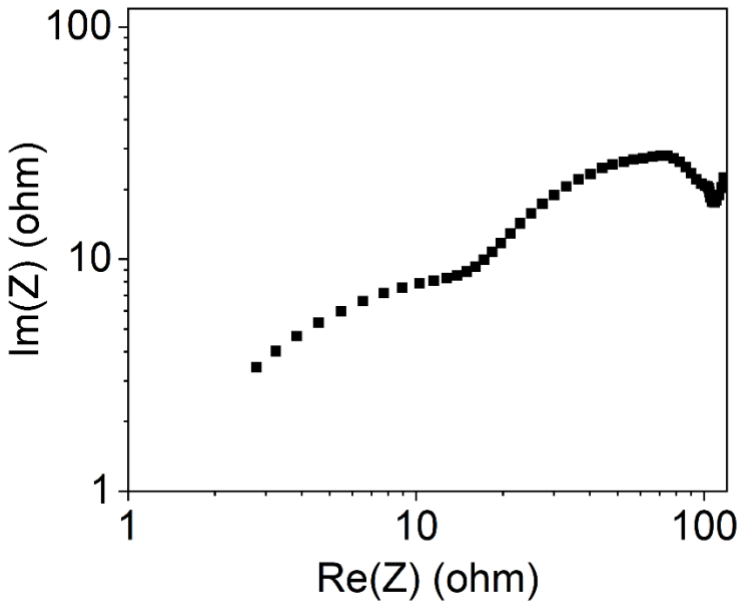

Figure S25 Nyquist plot of 8-layer su-pG300 FSSC.

Table S1 The capacitance and cycling life of 3D-tsSC300 with current studies.

Material Name	Electrolyte	Capacitance (F/g)	Current Density (A/g)	Cycle Number	Capacitance Retention %	REF
This Work	1.0 M H_2SO_4	157.6	10	15000	97.41	
cc-AT/CNT	1.0 M H_2SO_4	284	21	20000	80	[1]
PANI/CNTs	0.2 M Na_2SO_4	410	15	5800	65	[2]
HPC/PANI	1.0 M Na_2SO_4	134	1	5000	91.6	[3]
Deciduous Trees	1.0 M H_2SO_4	24	0.25	10000	100	[4]
Palm Kernel Shell	1.0 M Na_2SO_4	47	0.5	3500	114	[5]
Olive Residues	1.0 M H_2SO_4	166	1	12500	100	[6]
Rice Straw	1.0 M H_2SO_4	190	10	5000	99	[7]
Corn Silk	6.0 M KOH	160	1	2500	92.5	[8]
Pineapple Leaf Fiber	1.0 M H_2SO_4	210	20	10000	86	[9]
BNO-GF	0.5 M H_2SO_4	289.6	2	10000	120	[10]
PCF-WPU	6 M KOH	74.4	0.1	5000	97.7 (3 A/g)	[11]
CMS-Co-ZIF-L	6 M KOH	238	1	10000	94.3	[12]
NiCo-LDH-NCF	2 M KOH	1512	0.5	10000	80.4 (5 A/g)	[13]
VArGO	6 M KOH	145	0.5	15000	94.8 (20 A/g)	[14]
rGO powder	6 M KOH	159	0.5			[14]

rGO film	6 M KOH	122	0.5			[14]
SHS@SC	PVA/LiCl gel	29.6	20 mA/cm2 (~0.3 mA/g)	3000	90.9 (.75 mA/g)	[15]
CNT/GP micro-conduits	1 M H_2SO_4	500	60 mA/cm2 (12.6 A/g)	10000	95	[16]
N-MFCNC900	1M H2SO4	352	5	2000	96.4 (20 A/g)	[17]
N,S-PCNs1-1	6M KOH	298	0.5	10000	98	[18]
P-HPC	6M KOH	133	10	10000	98	[19]

Reference

1 X. Chang, C. W. Lin, A. Huang, M. F. El-Kady and R. B. Kaner, *Nano Lett.*, 2023, **23**, 3317–3325.

2 S. Hussain, E. Kovacevic, R. Amade, J. Berndt, C. Pattyn, A. Dias, C. Boulmer-Leborgne, M. R. Ammar and E. Bertran-Serra, *Electrochim. Acta*, 2018, **268**, 218–225.

3 P. Yu, Z. Zhang, L. Zheng, F. Teng, L. Hu and X. Fang, *Adv. Energy Mater.*, 2016, **6**, 1–10.

4 A. Jain, M. Ghosh, M. Krajewski, S. Kurungot and M. Michalska, *J. Energy Storage*, 2021, **34**, 102178.

5 I. I. Misnon, N. K. M. Zain and R. Jose, *Waste and Biomass Valorization*, 2019, **10**, 1731–1740.

6 A. Elmouwahidi, E. Bailón-García, A. F. Pérez-Cadenas, F. J. Maldonado-Hódar and F. Carrasco-Marín, *Electrochim. Acta*, 2017, **229**, 219–228.

7 N. Sudhan, K. Subramani, M. Karnan, N. Ilayaraja and M. Sathish, *Energy and Fuels*, 2017, **31**, 977–985.

8 T. Mitravinda, K. Nanaji, S. Anandan, A. Jyothirmayi, V. S. K. Chakravadhanula, C. S. Sharma and T. N. Rao, *J. Electrochem. Soc.*, 2018, **165**, A3369–A3379.

9 T. Meekati, P. Pakawatpanurut, T. Amornsakchai, N. Meethong and J. Sodtipinta, *J. Energy Storage*, 2023, **71**, 108135.

10 F. Lu, W. Kong, K. Su, P. Xia, Y. Xue, X. Zeng, X. Wang and M. Zhou, *Chem. Eng. Sci.*, 2023, **265**, 118232.

11 M. Udayakumar, P. Tóth, H. Wiinikka, J. S. Malhotra, B. Likozar, S. Gyergyek, A. K. Leskó, R. Thangaraj and Z. Németh, *Sci. Rep.*, 2022, **12**, 1–14.

12 M. Cao, Y. Feng, R. Tian, Q. Chen, J. Chen, M. Jia and J. Yao, *Carbon N. Y.*, 2020, **161**, 224–230.

13 Y. Liu, Y. Wang, C. Shi, Y. Chen, D. Li, Z. He, C. Wang, L. Guo and J. Ma, *Carbon N. Y.*, 2020, **165**, 129–138.

14 Y. Yoon, K. Lee, S. Kwon, S. Seo, H. Yoo, S. Kim, Y. Shin, Y. Park, D. Kim, J. Y. Choi and H. Lee, *ACS Nano*, 2014, **8**, 4580–4590.

15 J. Shang, Q. Huang, L. Wang, Y. Yang, P. Li and Z. Zheng, *Adv. Mater.*, 2020, **32**, 1–9.

16 G. Xiong, P. He, Z. Lyu, T. Chen, B. Huang, L. Chen and T. S. Fisher, *Nat. Commun.*, , DOI:10.1038/s41467-018-03112-3.

17 X. Wu, Z. Shi, R. Tjandra, A. J. Cousins, S. Sy, A. Yu, R. M. Berry and K. C. Tam, *J. Mater. Chem. A*, 2015, **3**, 23768–23777.

18 Y. Li, G. Wang, T. Wei, Z. Fan and P. Yan, *Nano Energy*, 2016, **19**, 165–175.
19 J. Yi, Y. Qing, C. T. Wu, Y. Zeng, Y. Wu, X. Lu and Y. Tong, *J. Power Sources*, 2017, **351**, 130–137.